SOCIETY FOR EXPERIMENTAL BIOLOGY

Journal of Experimental Botany, Vol. 72, No. 2 pp. 459–475, 2021
doi:10.1093/jxb/eraa485 Advance Access Publication 17 October 2020
This paper is available online free of all access charges (see https://academic.oup.com/jxb/pages/openaccess for further details)

RESEARCH PAPER

Endogenous indole-3-acetamide levels contribute to the crosstalk between auxin and abscisic acid, and trigger plant stress responses in Arabidopsis

Marta-Marina Pérez-Alonso[1], Paloma Ortiz-García[1], José Moya-Cuevas[1], Thomas Lehmann[2], Beatriz Sánchez-Parra[1,*], Robert G. Björk[3,4], Sazzad Karim[5,6], Mohammad R. Amirjani[5,†], Henrik Aronsson[5], Mark D. Wilkinson[1] and Stephan Pollmann[1,7,‡]

[1] Centro de Biotecnología y Genómica de Plantas, Universidad Politécnica de Madrid (UPM) – Instituto Nacional de Investigación y Tecnología Agraria y Alimentaria (INIA), 28223 Pozuelo de Alarcón, Spain
[2] Lehrstuhl für Pflanzenphysiologie, Ruhr-Universität Bochum, 44801 Bochum, Germany
[3] Department of Earth Sciences, University of Gothenburg, 40530 Gothenburg, Sweden
[4] Gothenburg Global Biodiversity Centre, 40530 Gothenburg, Sweden
[5] Department of Biological and Environmental Sciences, University of Gothenburg, 40530 Gothenburg, Sweden
[6] Department of Infectious Diseases, Institute of Biomedicine, The Sahlgrenska Academy, University of Gothenburg, 40530 Gothenburg, Sweden
[7] Departamento de Biotecnología-Biología Vegetal, Escuela Técnica Superior de Ingeniería Agronómica, Alimentaria y de Biosistemas, Universidad Politécnica de Madrid (UPM), 28040 Madrid, Spain

* Current address: Max-Planck-Institute for Chemistry, Mainz, Germany.
† Current address: Department of Biology, Arak University, Arak, Iran.
‡ Correspondence: stephan.pollmann@upm.es

Received 4 September 2020; Editorial decision 9 October 2020; Accepted 13 October 2020

Editor: Richard Napier, University of Warwick, UK

Abstract

The evolutionary success of plants relies to a large extent on their extraordinary ability to adapt to changes in their environment. These adaptations require that plants balance their growth with their stress responses. Plant hormones are crucial mediators orchestrating the underlying adaptive processes. However, whether and how the growth-related hormone auxin and the stress-related hormones jasmonic acid, salicylic acid, and abscisic acid (ABA) are coordinated remains largely elusive. Here, we analyse the physiological role of AMIDASE 1 (AMI1) in Arabidopsis plant growth and its possible connection to plant adaptations to abiotic stresses. AMI1 contributes to cellular auxin homeostasis by catalysing the conversion of indole-acetamide into the major plant auxin indole-3-acetic acid. Functional impairment of AMI1 increases the plant's stress status rendering mutant plants more susceptible to abiotic stresses. Transcriptomic analysis of *ami1* mutants disclosed the reprogramming of a considerable number of stress-related genes, including jasmonic acid and ABA biosynthesis genes. The *ami1* mutants exhibit only moderately repressed growth but an enhanced ABA accumulation, which suggests a role for AMI1 in the crosstalk between auxin and ABA. Altogether, our results suggest that AMI1 is involved in coordinating the trade-off between plant growth and stress responses, balancing auxin and ABA homeostasis.

Keywords: Abiotic stress, abscisic acid, *Arabidopsis thaliana*, auxin biosynthesis, plant development, plant hormone crosstalk, indole-3-acetamide, indole-3-acetic acid

Abbreviations: ABA, abscisic acid; AMI, amidase; IAA, indole-3-acetic acid; IAM, indole-3-acetamide; IAOx, indole-3-acetaldoxime

Introduction

A constantly changing and often adverse environment represents a steady challenge to plants. These challenges include various biotic and abiotic stresses, such as pathogen infection, herbivory, high salinity, drought, or temperature changes (Spoel and Dong, 2008; Verma *et al*., 2016). In order to survive and secure their reproduction, plants often restrict their growth and development under adverse conditions, because energy resources are limited, and their allocation must be tightly balanced to meet the requirements of both growth and adaptive stress responses. To keep track with specific environmental demands, plants have evolved a complex hormone-based network to control their development in response to given changes in their surroundings. Using this system, they can shape their body plan and optimize their metabolism in accordance with prevailing environmental conditions.

Key determinants of this regulatory network are limited number of signaling molecules referred to as plant hormones. They orchestrate plant growth and development mainly by influencing the transcriptome of responding cells and organs, respectively. Plant hormones act in a combinatorial manner to produce a large number of different responses that are dependent not only on the perceived stimulus, but also on the specific properties of the responding tissue (Depuydt and Hardtke, 2011; Voß *et al*., 2014). There is mounting evidence for the involvement of auxin in the trade-off between growth and defense. For example, the transcription factor MYC2, which controls the expression of jasmonic acid (JA) responsive genes (Kazan and Manners, 2013), has been reported to negatively regulate the expression of *PLETHORA* (*PLT1* and *PLT2*) transcription factor genes, which control stem cell development and auxin biosynthesis in roots (Pinon *et al*., 2013). Other studies also revealed that auxin production is increased by JA through the induction of *ANTHANILATE SYNTHASE 1* (*ASA1*) and a small number of *YUCCA* genes in certain plant tissues (Sun *et al*., 2009; Hentrich *et al*., 2013).

Plants also balance their growth with responses to abiotic stresses (Zhu, 2002; Verma *et al*., 2016). When exposed to drought or high salinity, two major abiotic stress factors in the field, plants reduce their growth rate, while stress-resistance mechanisms are initiated. Through the flexible reprogramming of their gene regulatory networks, plants strive for the best suited phenotype for the prevailing stress condition (Claeys and Inzé, 2013; Julkowska and Testerink, 2015). Brassinosteroid signaling pathways are reported to contribute to the control of plant growth under drought or starvation stress by regulating autophagy (Nolan *et al*., 2017). However, other plant hormones including auxin and abscisic acid (ABA) are also assumed to contribute to the coordination of the growth–stress response trade-off. Auxin is known to be the crucial determinant for plant growth (Davies, 2010), whereas ABA is reported to operate as a stress hormone in responses to abiotic stimuli (Gomez-Cadenas *et al*., 2015; Ma *et al*., 2018).

Under optimal conditions, plants usually grow rapidly with their energy resources mainly dedicated to primary growth, including root system and leaf expansion, shoot elongation, and reproduction. In this scenario, auxin is pivotal because it governs virtually all aspects of plant growth and development through the promotion of cell elongation, expansion, and differentiation (Vanneste and Friml, 2009). To ensure optimal plant growth, auxin homeostasis needs to be tightly regulated (Ljung, 2013). In order to control cellular auxin contents, plants possess a series of different biochemical and biological tools, including *de novo* biosynthesis, inactivation through conjugation, sequestration, and degradation (Ruiz Rosquete *et al*., 2012; Brumos *et al*., 2018). In contrast, when plants are subjected to biotic and abiotic stresses, they respond with the adjustment of their growth program, which in many cases results in reduced growth rates and premature phase transition from vegetative to reproductive growth (Silva *et al*., 2013; Suzuki *et al*., 2014; Perdomo *et al*., 2015). JA and ABA, two well-characterized plant stress hormones, play crucial roles in plant responses to biotic and abiotic stress factors. However, an underlying mechanism by which these two phytohormones are connected with cellular auxin levels remains largely elusive.

Mainly based on *in vitro* evidence, AMIDASE 1 (AMI1) has been suggested to act in a side pathway of indole-3-acetic acid (IAA) biosynthesis (Fig. 1), converting indole-3-acetamide (IAM) into IAA (Pollmann *et al*., 2003; Neu *et al*., 2007; Nemoto *et al*., 2009; Sánchez-Parra *et al*., 2014). In Arabidopsis, the majority of IAM (95%) has been reported to derive from the precursor indole-3-acetaldoxime (IAOx) (Sugawara *et al*., 2009). The enzyme responsible for the biochemical conversion, however, has yet to be identified. IAOx depleted mutant plants, i.e. *cyp79b2 cyp79b3*, show neither significant alterations of free auxin contents under standard conditions nor transcriptional induction of other auxin biosynthesis pathway components to compensate the loss of IAOx-dependent pathway(s) (Zhao *et al*., 2002; Lehmann *et al*., 2017). Together, these findings argue against a contribution of AMI1 in general auxin biosynthesis. Here, we report the functional characterization of AMIDASE 1 (AMI1) *in vivo*. The comprehensive analysis of *AMI1* gain- and loss-of-function mutants provided indication for an involvement of AMI1 in auxin homeostasis. A loss of *AMI1* results in increased IAM levels and moderately reduced IAA contents, whereas conditional overexpression of *AMI1* (AMI1ind) had the opposite effect. The examined *ami1* mutant alleles, *ami1-1* and *ami1-2*, show moderate growth reductions, while independent AMI1ind lines are characterized by auxin overproduction-related phenotypes. Comprehensive microarray analyses comparing *AMI1* mutants with wild-type (WT) plants revealed a tight connection of *AMI1* with various biotic and abiotic stresses, as numerous stress marker genes appeared to be differentially expressed. Abiotic stress treatments confirmed that *ami1* mutants are more susceptible towards osmotic stress. In summary, our results suggest that AMI1 is involved in

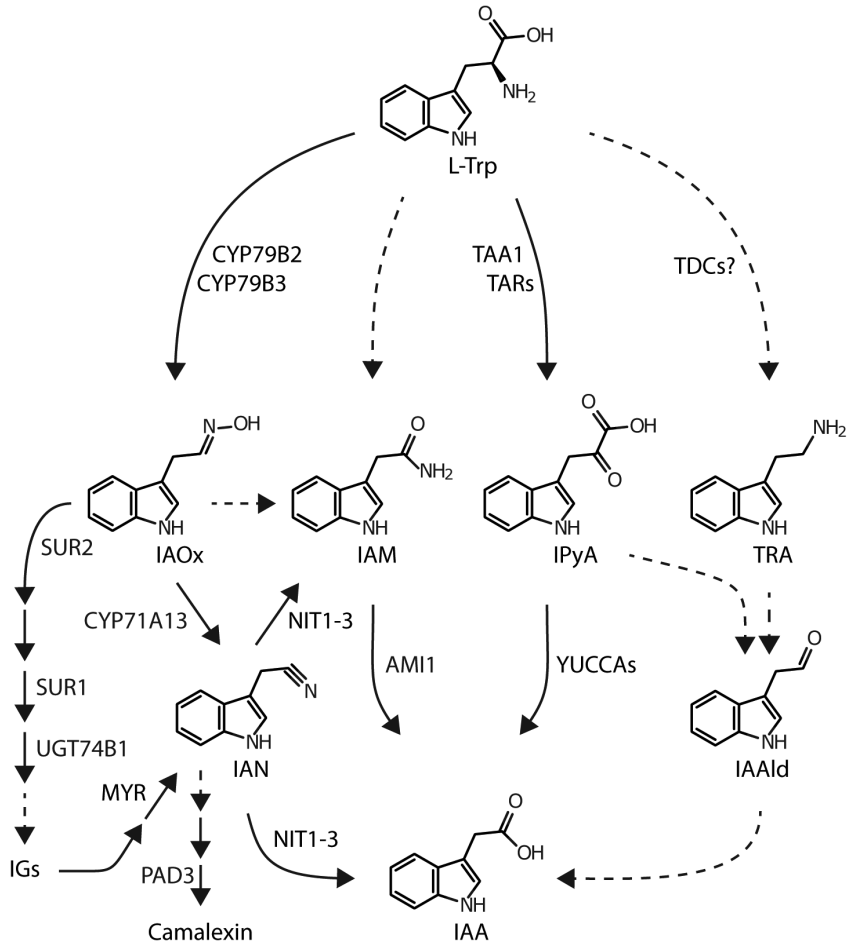

Fig. 1. Proposed anabolic routes for IAA biosynthesis in Arabidopsis. Dashed lines represent assumed reaction steps for which the corresponding genes/enzymes have not yet been identified. AMI1, AMIDASE 1; CYP71A13, CYTOCHROME P450 MONOOXYGENASE 71A13; CYP79B2/B3, CYTOCHROME P450 MONOOXYGENASE 79B2/B3; IAA, indole-3-acetic acid; IAAld, indole-3-acetaldehyde; IAM, indole-3-acetamide; IAN, indole-3-acetonitrile; IAOx, indole-3-acetaldoxime; IGs, indole glucosinolates; IPyA, indole-3-pyruvic acid; L-Trp, L-tryptophan; MYR, MYROSINASE; NIT1-3, NITRILASE 1-3; PAD3 PHYTOALEXIN DEFICIENT 3 (CYTOCHROME P450 MONOOXYGENASE 71B15); SUR1, SUPERROOT 1 (S-ALKYL-THIOHYDROXYMATE LYASE); SUR2, SUPERROOT 2 (CYTOCHROME P450 MONOOXYGENASE 83B1); TAA1, TRYPTOPHAN AMINOTRANSFERASE OF ARABIDOPSIS 1; TAR, TRYPTOPHAN AMINOTRANSFERASE RELATED; TDC, TRYPTOPHAN DECARBOXYLASE; TRA, tryptamine; UGT74B1, UDP-GLUCOSYL TRANSFERASE 74B1.

the coordination of the trade-off between growth and stress resistance, rather than in the *de novo* biosynthesis of auxin.

Materials and methods

Plant material and plant growth conditions

The experiments were carried out using Arabidopsis ecotype Col-0 (from Nottingham Arabidopsis Stock Centre (NASC), stock N1092). Seeds for *35S::tms2* (N6265), and the T-DNA insertion lines for *AMI1* (At1g08980; *ami1-2* (SALK_019823C)) were obtained from the Nottingham Arabidopsis Stock Centre, or kindly provided by Dr Henrik Aronsson, *ami1-1* (Aronsson *et al*., 2007). T-DNA mutants were genotyped according to Alonso *et al*. (2003). Primers for genotyping are given in Supplementary Table S1 at *JXB* online. If not stated otherwise, seedlings were raised under sterile conditions on solidified ½ MS medium containing 1% (w/v) sucrose in Petri dishes (Murashige and Skoog, 1962). Plantlets were kept under constant environmental short day (SD) conditions (8 h light at 24 °C, 16 h darkness at 20 °C, 105 µmol photons m^{-2} s^{-1} photosynthetically active radiation) for 2–3 weeks. If older plant material was used, the plant organs were harvested from plants grown in a greenhouse on a mixture of soil and sand (2:1) for 4–6 weeks in SD conditions. Thereafter, plants were transferred to long day (LD) conditions (16 h photoperiod). The greenhouse was maintained under constant climatic conditions, 22–24 °C during the daytime and 18–20 °C overnight. The photosynthetically active radiation was no less than 150 µmol photons m^{-2} s^{-1}. Expression of the transgene in AMI1ind lines was induced by either 10 µM β-estradiol added to the growth medium or by the administration of 50 µM β-estradiol through irrigation. In all experiments that employed AMI1ind lines, corresponding WT control plants were also grown on medium containing β-estradiol.

Generation of transgenic plants

Transgenic plants conditionally overexpressing AMI1 with an N-terminal *c-myc* tag (AMI1ind) and containing AMI1 promoter reporter constructs (*pAMI1::GUS*), respectively, were generated as

described in the following. In the first place, Gateway-compatible entry and destination vectors were produced. To do so, the attL-cassette from pENTR1a (Thermo Fisher Scientific) was amplified by PCR using the primers pSP-ENTR1-For-NheI and pSP-ENTR1-Rev-HindIII, thereby adding *Nhe*I and *Hin*dIII sites. After cloning into pGEM-T and sequencing, the *Nhe*I/*Hin*dIII fragment was integrated into pASK-IBA5 (IBA), giving rise to an ampicillin-selectable entry vector (pSP-ENTR1). For the preparation of promoter reporter constructs, we cloned the *Xba*I/*Sac*I *uid*A fragment from pGPTV-BAR (Becker *et al.*, 1992) into pSP-ENTR1 (pSP-ENTR2). To generate a suitable destination clone, we integrated the Gateway conversion cassette (Thermo Fisher Scientific) into the *Hin*dIII/*Sac*I sites of pGPTV-BAR, yielding a Gateway-compatible binary vector (pSP-DEST1), which facilitates BASTA selection. Next, the genomic DNA fragment, starting after the stop codon of the 5′ upstream gene (At1g08970) and reaching to the middle of the third exon of the *AMI1* gene, was amplified using the primers AMI1-PRlong-NotI-NcoI and AMI1-Ex3-Rev-SmaI and cloned into pBluescript SK(+) for sequence analysis. Thereafter, the promoter fragment was integrated into pSP-ENTR2 by using the added *Nco*I/*Sma*I sites. Thereby, a translational fusion with the β-glucuronidase gene (*uid*A) in pSP-ENTR2 was generated, resulting in the construct pSP-ENTR2-AMI1-GUS. The incorporated intergenic fragment between the stop codon of At1g08970 and the *AMI1* start codon had a length of 615 base pairs. The final binary vector, pSP-AMI1-PromA, was generated by homologous recombination, incorporating the Gateway cassette included in pSP-ENTR2-AMI1-GUS into pSP-DEST1 using the Gateway LR Clonase II mix (Thermo Fisher Scientific).

We next added a 5′ myc-tag extension to the *AMI1* cDNA by PCR amplification. The PCR product was integrated into pGEM-T and the sequence integrity was verified. In order to construct an inducible *AMI1* plant expression system, the *myc*:*AMI1* fragment was integrated into pSP-ENTR1, yielding the vector pENTR-AMI1ind. Using the Gateway LR Clonase II mix, recombination of pENTR-AMI1ind with the destination vector pMDC7, a Gateway-compatible pER8 derivate (Zuo *et al.*, 2000), created the binary vector pER-AMI1ind in which conditional *AMI1* expression is facilitated by the β-estradiol inducible XVE transactivator. Correct integration of the target sequences in all resulting binary vectors was verified by PCR. Sequence information on the employed primer can be found in Supplementary Table S1. All constructs were transformed into Arabidopsis WT (Col-0) by *Agrobacterium*-mediated transformation (Clough and Bent, 1998). T_1 seeds were harvested, sown on half-strength MS medium (0.8% phytoagar and 1% sucrose) adding either 5 mg l^{-1} BASTA (Hoechst) (pSP-AMI1-PromA) or 15 μg ml^{-1} hygromycin (pER-AMI1ind) to select transformants. In all subsequent experiments only selected T_3 seeds were used.

Transcriptomics

Total RNA was extracted from 100 mg plant tissue as previously described (Oñate-Sánchez and Vicente-Carbajosa, 2008). Labeling and hybridization of cDNA libraries from *ami1-2*, AMI1ind-2, and Col-0 to ATH1 DNA chips (Affymetrix) was performed by the CNB Genomics Service (Madrid, Spain). For each genotype three biological replicates were processed. Variation between replicates was accounted for by using the LIMMA model (Ritchie *et al.*, 2015). Differentially expressed genes were identified by a modified *t*-test implemented in the LIMMA package. A Benjamini–Hochberg correction was used to adjust for multiple testing. An adjusted *P*-value <0.05 and fold-change ≥1.5 were arbitrarily chosen to select 378 and 878 differentially expressed genes (DEGs) in *ami1-2* and AMI1ind-2, respectively, relative to WT (see Supplementary Table S2). The Gene Set Enrichment Analysis (GSEA) used a hypergeometric test with a Benjamini–Hochberg false discovery rate (FDR) correction and a post-correction selection significance level of $P<0.05$ (Maere *et al.*, 2005). Complementing the GSEA, parametric analysis of gene set enrichment (PAGE) analyses were carried out to determine GO terms enriched in the de-regulated gene groups. The PAGE method is statistically more sensitive and accounts for both the number of genes and their respective expression patterns, employing a Benjamini–Hochberg (FDR) multi-test adjustment and a significance of $P<0.05$ (Kim and Volsky, 2005).

Selected transcripts were validated in independent experiments by qRT-PCR. For each genotype and condition, total RNA from three independent biological replicates was harvested and analysed in triplicate (technical replicates). First-strand synthesis was performed according to the supplier's instructions, using M-MLV reverse transcriptase and oligo$(dT)_{15}$ primer (Promega). Two nanograms of cDNA was used as template for qPCR, which was performed according to the manufacturer's instructions using the FastStart SYBR Green Master solution (Roche Diagnostics) on a Lightcycler 480 Real-Time PCR system (Roche Diagnostics). Relative quantification of expression was calculated after data analysis by the Lightcycler 480 software (Roche Diagnostics), using the comparative $2^{-\Delta\Delta CT}$ method (Livak and Schmittgen, 2001) with *APT1* (At1g27450) and *UBQ10* (At4g05320) as reference genes (Czechowski *et al.*, 2005; Jost *et al.*, 2007). See Supplementary Table S1 for primer sequences.

Assay for β-glucuronidase activity

Histochemical β-glucuronidase (GUS) assays were performed as described by Jefferson *et al.* (1987). Seedlings and detached plant parts were respectively infiltrated with a GUS staining solution, consisting of 1 mM 5-bromo-4-chloro-3-indoxyl-β-D-glucuronic acid (X-Gluc), 50 mM potassium phosphate buffer, pH 7.0, 1 mM EDTA, and 0.1% Triton X-100, and incubated for 16 h at room temperature. Chlorophyll was removed by washing with an ethanol series (30%, 70%, and 96%), and the tissue was rehydrated in water for photography. For the fluorometric quantification of GUS activity, 4-methylumeliferyl-β-D-glucuronide (4-MUG) was used as substrate, which yields the fluorescent molecule 4-methylumbelliferone (4-MU) as product (Gallagher, 1992). To this end, 100 mg of hormone or mock-treated seedlings was transferred into 200 μl GUS extraction buffer (50 mM $NaHPO_4$, pH 7.0, 10 mM β-mercaptoethanol, 10 mM Na_2EDTA, pH 8.0, 0.1% sarcosyl (v/v), 0.1% Triton X-100 (v/v)) and fully homogenized. After a 2 min centrifugation at 14 500 *g*, 100 μl of the supernatants were transferred to a 48-well plate and 100 μl of 4 mM 4-MUG was added to each well. Samples were incubated for 5 min at 37 °C in the dark, before the reaction was stopped by adding 100 μl 200 mM Na_2CO_3 (T_0 GUS activity). The procedure was repeated, but with an extended incubation time of 60 min (T_{60} GUS activity). The fluorescence was measured at 360 nm excitation and 460 nm emission (automatic gain, 50% mirror) using a TECAN Genios Pro fluorescence spectrometer (MTX Lab Systems).

GUS activity was calculated as follows:

$$\text{GUS activity}\ \left(\text{pmol}\ /\ \text{min}^{-1}\right) = \frac{\Delta F \cdot 10^{-1}}{t}$$

with ΔF giving the fluorescence intensity $T_{60}-T_0$, 10 referring to the fluorescence units corresponding to 1 pmol of hydrolysed 4-MUG, and t representing the incubation time in minutes. GUS activity expressed in units was activity per mg of protein, where the protein amount was quantified using the Bradford method (Bradford, 1976).

Amidase activity assay

The IAM hydrolase activity in plants was determined as previously described (Neu *et al.*, 2007). In brief, crude extracts from 2-week-old seedlings were prepared. One hundred milligrams of plant tissue was shock-frozen in liquid nitrogen. The tissue was disrupted using micropestles. As the material started to thaw, buffer (50 mM HEPES, pH 8.5, 200 mM sucrose, 3 mM EDTA, 3 mM DTT, 5% (w/v) insoluble polyvinylpyrrolidone) was added in a ratio of 1:3 (w/v). The suspension was

homogenized until no more tissue fragments were visible. Cell debris and insoluble matter were collected by centrifugation (16 000 *g*, 15 min, 4 °C) and the supernatant was transferred to fresh tubes. Protein concentrations were determined according to Bradford (1976), using serum albumin as a protein standard. Aliquots containing 200 µg of protein were incubated with 5 mM IAM in a total volume of 300 µl of 50 mM potassium phosphate buffer (pH 7.5) for 3 h at 30 °C. Finally, the amount of IAA produced was quantified by reverse phase HPLC. The data were analysed using Student's *t*-test to compare two means. Statistical analyses were conducted using Prism version 7.0a (GraphPad Software).

IAA and IAM quantification

The LC-MS analysis of endogenous IAA and IAM was carried out according to Novák *et al.* (2012). For each sample 100 mg of plant material was harvested and immediately frozen in liquid nitrogen. Each independent experiment used at least three biological replicates. Sample handling times were kept as short as possible to prevent distortion of the IAA pool through the autocatalytic decay of precursor molecules (Gélinas-Marion *et al.*, 2020). The plant material was transferred into 2 ml screw-cap tubes filled with ceramic beads (MagNA Lyser Green Beads; Roche Diagnostics) and endogenous IAA and IAM was extracted into 1 ml of cold potassium phosphate buffer (50 mM, pH 7.0) containing 1% diethyldithiocarbamic acid sodium salt and 50 pmol of the internal standards [$^2H_5$]IAA and [$^2H_5$,^{15}N]IAM (OlchemIm). The plant material was crushed in a MagNA Lyser Instrument (Roche Diagnostics) at 8000 *g* for 1 min. After centrifugation (5 min, 16 000 g at 4 °C), 750 µl of the supernatants was transferred into fresh tubes and the pH adjusted to 2.7 with 1 M hydrochloric acid. Thereafter, samples were loaded onto Oasis™ HLB columns (1 ml, 30 mg; Waters Corp.) conditioned with 1 ml methanol and 1 ml water and equilibrated with 1 ml acidified sodium phosphate buffer (50 mM, pH 2.7). The columns were washed twice with 1.5 ml 5% methanol and subsequently eluted with 2 ml 80% methanol. The eluates were taken to dryness *in vacuo*. Prior to the mass spectrometric analysis, the evaporated samples were dissolved in 45 µl methanol with 0.1% formic acid (v/v). Ten microliters of the extract was separated using an Ultimate3000 RSLC system (Dionex), and analysed using a microTOF-Q II mass spectrometer (Bruker Daltonics). Analyte separation utilized a 50 mm×2.1 mm i.d., 1.7 µm, Acquity UPLC BEH C18 column with a 5 mm×2.1 mm i.d. Acquity UPLC BEH C18 VanGuard pre-column, and a 0.2 µm×2.1 mm i.d. in-line filter (Waters Corp.). The following binary gradient was applied: 0–2 min isocratic 98% solvent A (water with 0.1% (v/v) formic acid), 2% B (acetonitrile with 0.1% (v/v) formic acid); 2–30 min linear gradient to 5% A, 95% B; at 30 min step gradient to 100% B; isocratic for 1 min. Thereafter, the column was set to 98% A, 2% B and conditioned for 2 min before the next injection. The flow rate was 400 µl min^{-1}. Eluted compounds were analysed using a microTOF-Q II mass spectrometer (Bruker Daltonics) operated in positive electrospray mode. Typical settings were as follows: capillary voltage, −4500 V; dry gas temperature, 200 °C; dry gas flow, 10 l min^{-1}; funnel, RF 200 Vpp. Ions were detected from m/z 50 to 1000 at a repetition rate of 2 Hz. The instrument was operated in multiple reaction monitoring mode. Mass calibration was performed using sodium formate clusters (10 mM solution of NaOH in 50/50% v/v isopropanol/water containing 0.2% formic acid). For data processing the DataAnalysis 4.0 software (Bruker Daltonics) was used. The following transitions were recorded to determine analyte contents: IAM, m/z=175.2→130.1; [$^2H_5$,^{15}N]IAM, m/z=181.2→135.1 (retention time, 6.3 min); IAA, m/z=176.2→130.1; [$^2H_5$]IAA, m/z=181.2→135.1 (retention time, 8.8 min). Quantification was achieved by comparing peak areas of the endogenous compounds with those of the internal standards. The data were analysed using Student's *t*-test to compare the mutant mean with the mean of the control. Statistical analyses were conducted using Prism version 7.0a.

ABA quantification

The ABA contents in 50 mg of 10-day-old sterilely grown Col-0 and *ami1* seedlings were determined using GC-MS/MS (Bruker Daltonics, Scion-TQ) analysis as previously described (Ramos *et al.*, 2018). Quantification was carried out using stable isotope-labelled [$^2H_6$]ABA as internal standard. Endogenous hormone contents were calculated from the signal ratio of the unlabeled over the stable isotope-containing mass fragment observed in measurements that have been performed in quintuplicate. The data were analysed with one-way ANOVA followed by a Tukey–Kramer *post hoc* test to allow for comparison among all means. Statistical analyses were conducted using Prism version 7.0a

Western blotting

Both SDS-PAGE and amidase immunoblots were carried out as described by Neu *et al.* (2007). A monoclonal α-myc antibody, clone 9.E10 (Evan *et al.*, 1985), was used as first antibody at a final dilution of 65 mg l^{-1}. As second antibody was used, a rabbit-anti-mouse-IgG (Promega) coupled with an alkaline phosphatase.

Biomass and root morphology analysis

For the analysis of the root morphology, five replicate Petri dishes with ½ MS agar medium (0.5% sucrose, w/v), containing 21–26 seedlings, were used for each line. The root system morphology of the seedlings was investigated using the WinRhizo™ image analysis software (Regent Instruments Inc.). The roots were scanned using a 600 dpi resolution STD1600+ scanner (Regent Instruments Inc.) while still attached to the dish. The images were analysed to identify various root system morphology parameters (Björk *et al.*, 2007), namely root length (cm), surface area (cm^2), number of branches (forks), and number of root tips. The shoot and the root systems were then separated and their dry weight determined using a Sartorius ultra-micro scale (Sartorius GmbH, Göttingen, Germany) after drying the individual parts at 70 °C for at least 48 h. Root-to-shoot ratio (R/S ratio), specific root length (SRL; mg DW^{-1} root), specific root area (SRA; m^2 kg DW^{-1} root), specific root tip density (tips g DW^{-1} root), root tip density (tips cm^{-1} root), specific branching density (forks g DW^{-1} root), and branching density (forks cm^{-1} root) were calculated for each genotype (Björk *et al.*, 2007). Differences in the root architecture were investigated using a MANOVA, which was followed by Tukey's HSD *post hoc* test for the genotype. Statistical analyses were conducted using SPSS 18.0 (SPSS Inc.).

Root growth response assay

The root growth response was analysed according to the protocol of Zimmerman and Hitchcock (1942). Plants were grown on ½ MS plates for 7 d before they were transferred onto medium supplemented with either 5 nM to 10 µM IAA (from 100 mM stock in methanol) or 10 nM to 200 µM IAM (from 100 mM stock in methanol). Plates were wrapped in gas-permeable surgical tape (BSN medical GmbH) and grown vertically under constant conditions for 2 weeks. Subsequently, the primary root length increase of at least 12 individual plants per treatment was determined. Differences in primary root elongation were analysed using Student's *t*-test to compare two means. Statistical analyses were conducted using Prism version 7.0a.

Results

The AMI1 *gene is generally expressed in proliferating tissues, but repressed during early stages of germination*

In our previous work, we performed microscopic experiments using AMI1–GFP fusion proteins and semi-quantitative

RT-PCR to investigate the subcellular localization and tissue specific expression of *AMI1*. The experiments revealed a mainly cytoplasmic localization and the expression of *AMI1* in proliferating tissues, such as young leaves and flowers (Pollmann *et al*., 2006*b*). Additional qPCR experiments confirmed the expression pattern for *AMI1* on a tissue-specific basis. *AMI1* expression was detected in all analysed samples. The expression in roots was, however, low compared with the levels in all other tissues. In adult plants, *AMI1* expression was highest in juvenile leaves and petioles; lower transcript levels were detected in stems and in flower buds (see Supplementary Fig. S1A).

To enable further examination of *AMI1* expression during plant development, we generated *pAMI1::GUS* promoter reporter lines. Since qPCR data pointed towards high *AMI1* expression in young seedlings, we monitored β-glucuronidase (GUS) activity in *pAMI1::GUS* lines between 26 h and 72 h after imbibition (Fig. 2A). The GUS staining showed an increasing *AMI1* promoter activity with the ongoing of seedling development. Starting after about 48 h in the cotyledons, GUS activity peaked 64 h after germination. The observed promoter activity matches considerably well with the previously determined IAM profile during seed germination and early seedling development (Pollmann *et al*., 2002; Hoffmann *et al*., 2010), pointing towards a rapid decline of IAM levels during early seedling development. At later stages, especially in the primary root, the expression slowly decreased, while in root tips a clear GUS activity remained detectable. The qPCR experiment provided further evidence for a substantial *AMI1* expression in leaves, petioles, and flower buds. For this reason, we analysed *AMI1* promoter activity during later stages of development. In cotyledons, expression was mainly detected in the vascular tissue and on the very tip of the leaf (Fig. 2B). In primary leaves, GUS staining was visible in the vascular tissue, at the tip of the leaf, and also in trichomes (Fig. 2C). During flower development, at developmental stage 15 (Smyth *et al*., 1990), strong activity was detected in the petioles, pedicels and receptacles, in the vasculature of the sepals, and at the end of the pistil including the stigma (Fig. 2D). Only low activity was visible in the filaments and anthers, whereas the petals showed no staining (Fig. 2D, E). In developing siliques, at stage 17, strong promoter activity was observed at the end of the pedicels and on both ends of the silique, whereas nearly no activity was found in the developing seeds and funiculi (Fig. 2F). Taken together, these results confirm the expression of *AMI1* in proliferating tissues, including young seedlings and developing flowers.

High levels of IAM induce AMI1 *gene expression*

Numerous previous studies already analysed the transcriptomic response towards IAA in Arabidopsis. The inspection of publicly available datasets, e.g. GSE631 and GSE42007 (Okushima *et al*., 2005; Lewis *et al*., 2013), demonstrated that most auxin homeostasis-related genes show no significant response to IAA (see Supplementary Table S2). Consistent over both datasets, only a small number of *Gretchen Hagen 3* (*GH3*) genes appear to be significantly induced by IAA. *GH3* genes encode IAA amidosynthases that catalyse the conjugation of free IAA to amino acids, thereby physiologically inactivating the plant hormone (Staswick *et al*., 2005). To investigate the response of *AMI1* towards the exogenous application of IAA and IAM in closer detail, we performed qPCR experiments on 2-week-old seedlings, which were treated for different periods of time with the indoles. Generally confirming the transcriptomic data, the application of IAA (20 μM) triggered only a weak repression ($\log_2 = -1.3 \pm 0.1$) of *AMI1* transcription. In contrast, the treatment with 20 μM IAM significantly induced the expression of *AMI1*. The transcriptional level of *AMI1* temporarily increased to reach a $\log_2$ value of 2.9 ± 0.3 at 2 h, only to return to a lower level after 3 h of IAM treatment (Fig. 3). The induction of *AMI1* gene expression by its putative substrate, IAM, suggests a function of AMI1 in the control of cellular IAM levels.

Perturbations of AMI1 *gene expression alter auxin contents and trigger auxin-related phenotypes*

To explore the role of AMI1 in auxin homeostasis, we took a complementary reverse genetics approach. First, we studied two independent mutant alleles for *AMI1*, carrying T-DNA insertions either in the fourth intron (*ami1-1*) (Aronsson *et al*., 2007) or in the sixth exon (*ami1-2*). The T-DNA insertion sites of *ami1-1* and *ami1-2* were confirmed by sequencing. In the case of *ami1-2*, the sequencing of the genomic DNA revealed a tandem T-DNA insertion (Fig. 4A). Homozygous plants were isolated and genotyped (Fig. 4B). Both null alleles were devoid of detectable amounts of full-length *AMI1* mRNA (see Supplementary Fig. S1B), which could also be validated by qPCR, demonstrating a lack of expression of the second half of the *AMI1* gene, containing the T-DNA insertions (Supplementary Fig. S1C). The results provided evidence that the T-DNA insertions in *ami1-1* and *ami1-2* result in the formation of truncated and likely functionally impaired transcripts.

The phenotypic alterations observed in the *ami1* alleles were only moderate. Areal plant parts showed a slight growth reduction, particularly when grown on soil for a longer period of time (Fig. 4C). A more detailed analysis of the root system morphology of *AMI1* mutants employing the WinRhizo™ image analysis software confirmed this observation and revealed a significantly reduced root branching and total root length and area, respectively, for both *ami1* alleles (see Supplementary Fig. S2). Although the phenotypic alterations were not pronounced, we asked whether the altered *AMI1* expression translates into detectable changes in the chemotype. To this end, we examined IAM hydrolase activity in the *ami1* alleles (Fig. 4D). In comparison with WT, the amidase activity

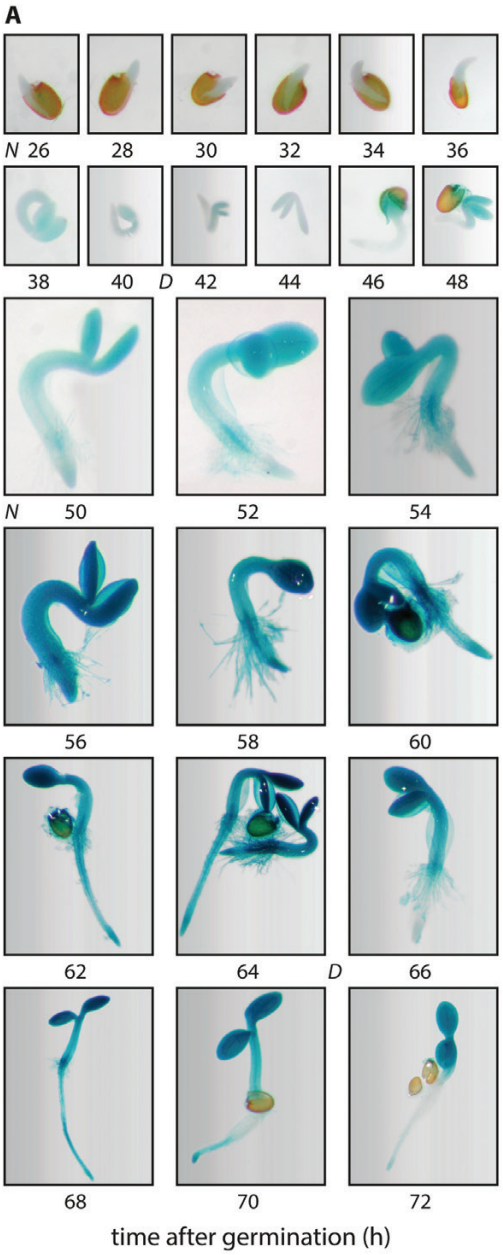

Fig. 2. Expression pattern of *AMI1* during plant development. (A) GUS staining of *pAMI1::GUS* seedlings 26–72 h after imbibition. Plants were grown on ½ MS medium under short day conditions (8 h light–16 h darkness) and then stained for reporter activity. The light–dark cycle is indicated by N (night) and D (day), respectively. (B) GUS staining of a 5-day-old cotyledon from a *pAMI1::GUS* seedling. Staining was observed at the cotyledon tip and in the vascular tissue. (C) GUS staining of a 6-week-old *pAMI1::GUS* leaf. Staining was located in the vascular tissue and at the tip of the leaf. (D) GUS staining of a mature flower from a *pAMI1::GUS* plant at developmental stage 15. Note the strong staining in the sepal vasculature, the pedicel, and on both ends of the carpel, including the stigma. (E) Magnification of a GUS stained anther from the flower shown in (D). (F) GUS staining of a developing silique at stage 17. Strong GUS activity can be observed at the ends of the siliques and at the end of the pedicel. The developmental stages of the flowers were classified according to Smyth *et al.* (1990).

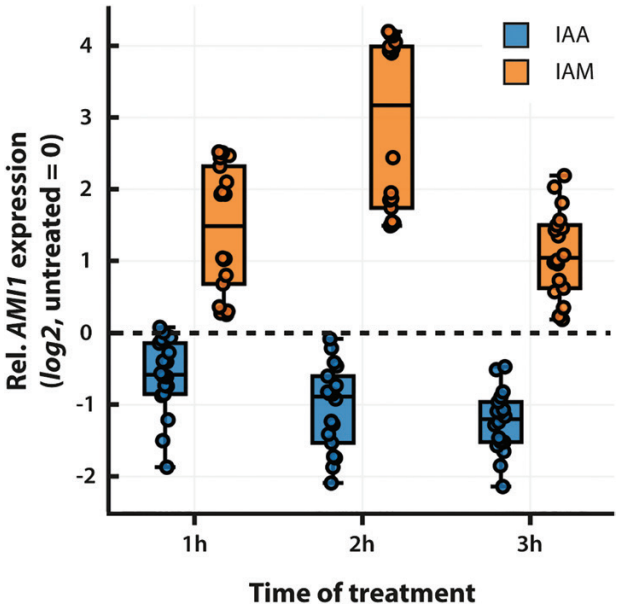

Fig. 3. Transcriptional response of *AMI1* towards exogenously applied IAA and IAM. Transcript levels of *AMI1* in treated seedlings were measured by qRT-PCR. One hundred milligrams of plant tissue was harvested for each sample after 1, 2, and 3 h of treatment with either 20 µM IAA or IAM and used for RNA extraction. Transcript abundance values are normalized to the geometric means of *APT1*, and *UBQ10* transcripts and given relative to *AMI1* expression levels in mock treated samples. Means are given with their SE (n=18). The dashed line reflects the *AMI1* expression level in mock treated control samples.

in *ami1-1* and *ami1-2* was not null but rather reduced by approximately 45–50%, pointing towards the existence of an additional IAM hydrolase in Arabidopsis. Next, we analysed changes in IAA and IAM contents by mass spectrometry. We found a correlation between the decreased IAM hydrolase activities in the *ami1* mutants and endogenous IAA and IAM levels. Both mutant alleles showed significantly reduced auxin contents, ranging from 15 to 30% under the WT level alongside with significantly higher IAM contents (Fig. 4E, F).

Secondly, we generated mutants conditionally overexpressing N-terminally *c-myc* tagged *AMI1* cDNA. In these lines, the *c-myc:AMI1* construct was under the control of the β-estradiol

inducible XVE transactivator (Zuo *et al.*, 2000). After screening numerous homozygous AMI1ind T_3-lines, two independent lines, AMI1ind-1 and AMI1ind-2, with considerable transgene expression (see Supplementary Fig. S3A) and significantly increased amidase activity (Fig. 4D) were selected for all following experiments. In contrast to the *ami1* alleles, 2-week-old AMI1ind lines displayed significantly higher IAA levels and nearly 60% less IAM relative to WT plants (Fig. 4E, F). However, the root system architecture of the AMI1ind lines resembled the WT (Supplementary Fig. S2A–C). To survey the influence of high-level *AMI1* expression on later stages of plant development, the AMI1ind mutants were grown on sterilized soil. Expression of the transgene was induced by irrigating the plants with water containing 50 μM β-estradiol (Supplementary Fig. S3A). In comparison with non-induced plants, the induced AMI1ind plants exhibited an auxin-related phenotype, showing retarded growth (Supplementary Fig. S3B) as well as curled leaf shapes (Supplementary Fig. S3C), reminiscent of other plants showing auxin overproduction (Zhao *et al.*, 2001; Zhang *et al.*, 2007; Hentrich *et al.*, 2013). Furthermore, the AMI1ind lines showed considerably accelerated flowering (Supplementary Fig. S3D).

To further characterize the impact of *AMI1* overexpression, we monitored the root growth in response to the suggested substrate of AMI1, IAM. AMI1ind lines and WT plants were grown on plates containing rising amounts of IAM (see Supplementary Fig. S4A). With rising concentrations, the growth inhibiting effect of IAM became more pronounced in AMI1ind plants relative to the WT. At 200 μM IAM, the primary root growth was nearly fully suppressed in AMI1ind. Under these conditions, the overexpressors carried predominantly adventitious roots on their hypocotyls. In contrast, WT seedlings grown in parallel were at least able to produce short primary roots with an increased number of lateral and adventitious roots. The described adventitious root phenotype at high IAM levels is in line with the phenotype previously observed for tobacco plants constitutively overexpressing the *Agrobacterium tumefaciens iaaM* and *iaaH* genes (Sitbon *et al.*, 1992).

To quantify the observed differences, primary root elongation responses towards IAM of AMI1ind, *ami1*, and *35S::tms2* were determined and compared with WT Arabidopsis (Fig. 5). The *35S::tms2* mutant served as a control to assess the effect of *AMI1* overexpression. The line contains the 35S-driven *INDOLEACETAMIDE HYDROLASE* (*tms2*) gene from *Agrobacterium tumefaciens* (Karlin-Neumann *et al.*, 1991). Seedlings of the different genotypes were grown on ½ MS plates for 7 d, before they were transferred to plates containing IAM. While *ami1-1* and *ami1-2* seemed to be less sensitive towards IAM in the medium (Fig. 5A), AMI1ind-1 and AMI1ind-2 primary roots exhibited an increased sensitivity towards IAM, manifesting in a significantly stronger repression of primary root elongation growth relative to WT plants. Resembling the root elongation response of *35S::tms2*, both AMI1ind lines exhibited reduced root growth with rising IAM contents. At very high IAM concentrations (100 μM), however, root elongation was equally suppressed in all tested seedlings (Fig. 5B). The auxin response of the *AMI1* gain-of-function mutants was also examined in a similar manner employing plates containing different amounts of IAA (see Supplementary Fig. S4B, C). Only at low IAA contents (0.01 μM), AMI1ind and *35S::tms2* seedlings showed significantly less primary root elongation, which might be attributable to the higher intrinsic IAA level in those lines. With higher concentrations of IAA (0.1–10 μM) the growth response of the mutant roots was indistinguishable from that of the WT control. Hence, it can be concluded that IAA perception is not affected by the conditional overexpression of *AMI1*. In summary, the metabolomic data underscore a contribution of AMI1 to auxin homeostasis. The only mild phenotype of the *ami1* mutants, however, implies that the role of the enzyme is likely not to be to control the general supply of auxin, but possibly to control the cellular IAM pool.

Altered abundance of salt-, osmotic-, and wounding-related transcripts in ami1-2

To obtain further information on the molecular alterations triggered by perturbations of *AMI1* gene expression, we conducted transcriptome profiling of sterilely grown 12-day-old WT, *ami1-2*, and AMI1ind-2 seedlings. Herein, we were especially interested in transcriptional changes of genes previously associated with auxin-related processes. Hence, we first analysed the differential expression of a sub-group of 128 genes, related with auxin biosynthesis, conjugation/deconjugation, degradation, transport, and signaling. The study revealed that only a very few of the tested genes were differentially expressed in the mutants (see Supplementary Table S2). Except for the induction of *YUC8* and *ILL5/IAR3*, no other auxin homeostasis-related genes appeared to be differentially expressed in *ami1-2*. YUC8 is involved in auxin biosynthesis (Hentrich *et al.*, 2013), and ILL5/IAR3 are two highly similar IAA–amino acid hydrolases, specific for IAA–Leu and IAA–Phe (Davies *et al.*, 1999; LeClere *et al.*, 2002). The induction of *YUC8* and *ILL5/IAR3* could possibly be conducive to compensating the loss of *AMI1* in auxin biosynthesis. On the other hand, *YUC8* and *ILL5/IAR3* have been associated with biotic stress responses (Truman *et al.*, 2010; Hentrich *et al.*, 2013), which could also suggest a link of AMI1 with plant stress-related processes. For AMI1ind-2, we found the auxin conjugation-related genes *UGT75D1* and *GH3.17* to be significantly induced. Together with the de-regulation of a number of auxin signaling and transport components, including *LAX2*, *PIN4*, *PIN5*, *IAA1*, *IAA12*, *IAA14*, *ARF6*, *ARF7*, and *ARF16*, this likely represents an answer to the overproduction of IAA in the conditional mutant.

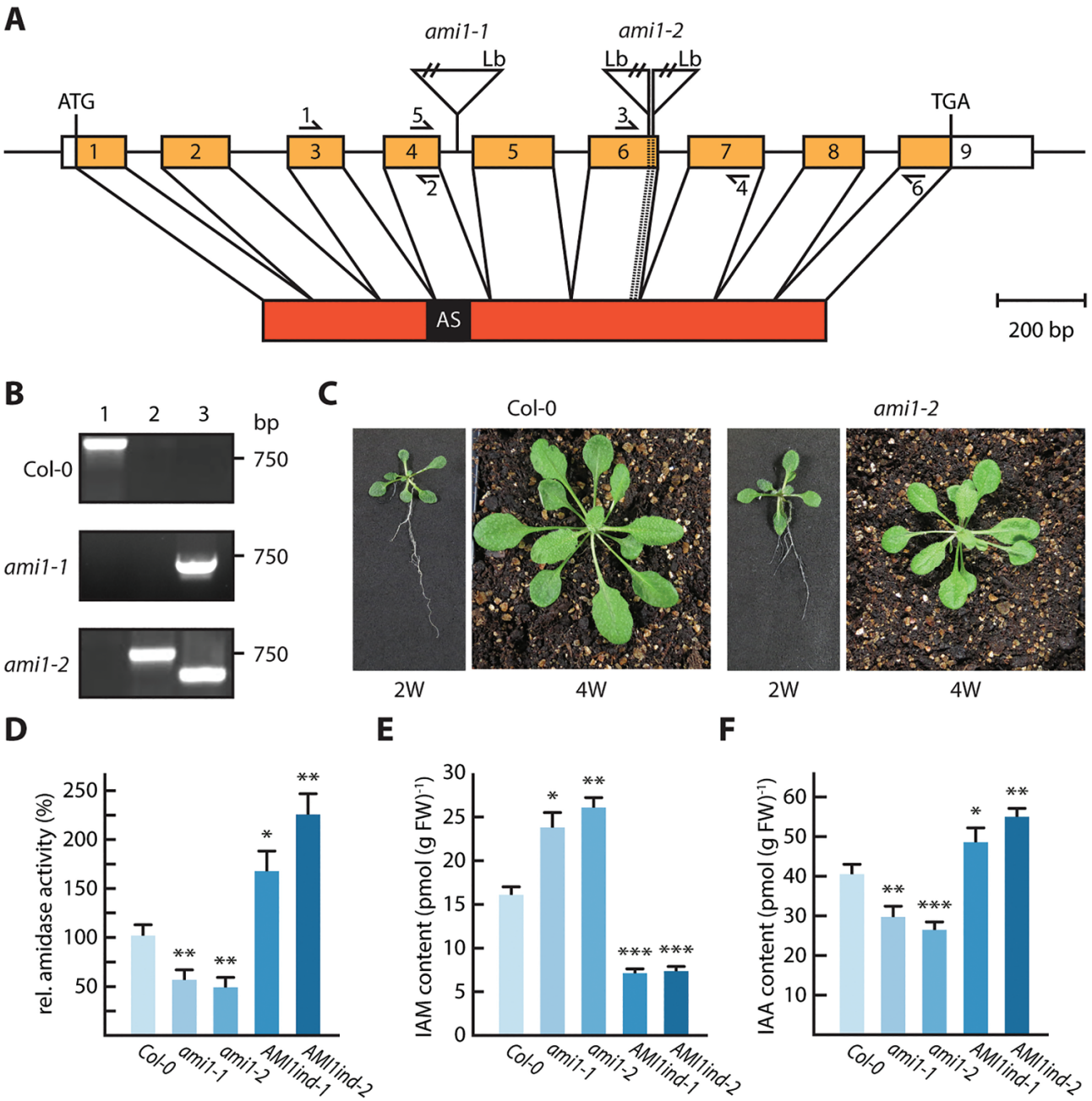

Fig. 4. Characterization of *ami1* T-DNA insertion lines. (A) Genomic *AMI1* region (At1g08980) showing the exon/intron structure and the T-DNA insertion sites in intron 4 and exon 6. The primer pairs used for either RT-PCR (1/2, 3/4) or qRT-PCR (5/6) are shown as arrows. The resulting cDNA with the fused exons, but without the 5′ and 3′ untranslated regions, is depicted below. Also given is the amidase signature (AS) domain of the derived protein. Insertion sites of the T-DNA in the alleles *ami1-1* and *ami1-2* were analysed by sequencing. Genomic sequence and cDNA, but not the T-DNA, are drawn to scale. Lb, left boarder; ATG, start codon; TGA, stop codon. (B) PCR zygosity analysis of the studied genotypes. Total genomic DNA was extracted from wild-type and homozygous T-DNA insertion lines. One T-DNA and two gene specific primers (Supplementary Table S1) were used in three combinations for genotyping: the first reaction (1) contained two gene-specific primers, flanking the T-DNA insertion; the second (2) comprised the T-DNA left border primer and the upstream gene specific primer; the third reaction (3) contained the T-DNA left border primer and the downstream gene specific primer. (C) Phenotype of Arabidopsis wild-type (Col-0) and *ami1-2* plants grown for either 2 weeks on ½ MS plates or 4 weeks on soil. (D) IAM hydrolase activity in *ami1* T-DNA insertion mutants and AMI1 overexpressing AMI1ind lines. Crude extracts were incubated for 3 h at 30 °C with 5 mM IAM as substrate. The IAA produced was detected after separation by reverse phase HPLC. Means ±SE are given (n=5). Similar results were obtained in two independent experiments. (E, F) Analysis of IAM (E) and free IAA (F) levels. Two-week-old seedlings were used for the determination of IAA and IAM by LC-MS analysis. Three independent biological replicates were assessed. Quantification of free IAA levels in *ami1-1*, *ami1-2*, AMI1ind-1, and AMI1ind-2 relative to the wild-type (Col-0). The standard error of the mean is given (n=9). Student's t-test: $^{*}P \leq 0.05$, $^{**}P \leq 0.01$, $^{***}P \leq 0.0001$.

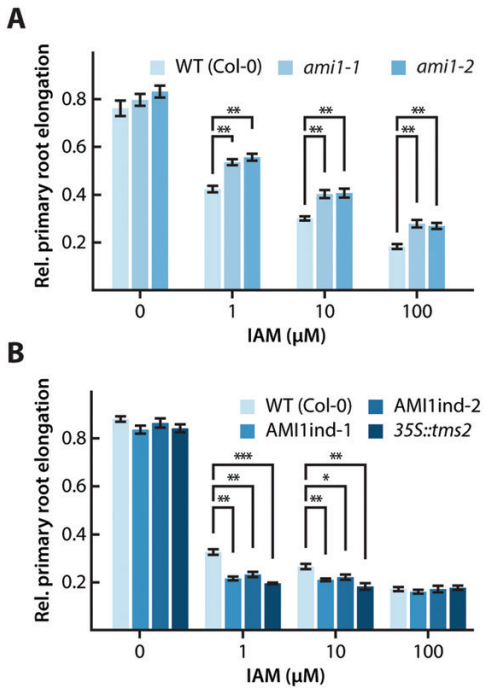

Fig. 5. Root growth response of *ami1* and AMI1ind mutants towards IAM. (A, B) Comparison of the root growth response of *ami1* knockout (A) and IAM amidohydrolase overexpressing (B) mutants with wild-type (WT) seedlings. Seeds were germinated and grown for 7 d on ½ MS plates, before they were transferred onto plates containing indicated amounts of either IAM or IAA. In order to examine the sensitivity toward IAM and IAA in the medium without the bias of initially shorter primary roots, the impact of the two compounds was expressed in relative terms. Therefore, the length of the longest primary root of each genotype grown under control conditions was set to a value of 1 and all other roots of the corresponding genotype were expressed relative to this value. The primary root elongation of seedlings was quantified. The expression of the transgene in the AMI1ind lines was induced by adding 10 μM β-estradiol to the plates. At least 16 seedlings of each genotype were measured for each condition. The data represent means ±SE. Asterisks indicate significant differences between the corresponding WT control and the tested genotypes under the described conditions. Student's *t*-test: $^{*}P \leq 0.05$, $^{**}P \leq 0.01$.

Next, we undertook a detailed profiling approach to obtain a broader overview of the transcriptomic alterations in the *AMI1* mutants. Based on an adjusted *P*-value of <0.05 and an arbitrarily chosen fold-change value of ≥1.5, 391 and 969 DEGs were selected in *ami1-2* and AMI1ind-2, respectively (see Supplementary Table S2). From these genes, 287 and 347 were up- and 88 and 622 were down-regulated in *ami1-2* and AMI1ind-2, respectively (Fig. 6A). From the DEGs, 289 and 775 genes, respectively, could be assigned to 178 and 273 significant GO terms for *ami1-2* and AMI1ind-2 (Supplementary Table S3).

Parametric analysis of gene set enrichment (PAGE) suggested a prominent de-regulation of plant stress response-related genes in the *AMI1* mutants. Among the up-regulated genes in *ami1-2*, we observed the enrichment of genes related with salt stress and osmotic stress, as well as oxylipin biosynthesis and signaling. The corresponding genes included, for instance, the AP2/ERF transcription factors *ERF53* and *RAP2.6*, the MYB transcription factors *MYB34*, *MYB47*, *MYB74*, *MYB102*, and *MYB108*, the JA signaling repressors *JAZ3* and *JAZ9*, *ALLENE OXIDE SYNTHASE* (*AOS*), *HYDROPEROXIDE LYASE* (*HPL1*), *JASMONIC ACID RESPONSE 1* (*JAR1*), the dehydration responsive genes *RD29A*, *ERD7*, and *EDR9*, as well as the 9-*cis*-epoxycarotenoid dioxygenase (NCED) gene *NCED3* (Fig. 6B; Supplementary Fig. S5). Among the down-regulated genes in AMI1ind-2, we found an over-representation of biotic and drought stress-related genes. This second group of genes included, among others, the transcription factors *WRKY33*, *ORA47*, *ZAT10*, *DREB1B*, and *DREB26*, as well as *PHENYL ALANINE AMMONIA LYASE 3* (*PAL3*), *MITOGEN ACTIVATED PROTEIN KINASE 3* (*MAPK3*), and the *RESPIRATORY BURST OXIDASE HOMOLOGUE D* (*RBOHD*) (Fig. 6C; Supplementary Fig. S5). Altogether, the transcriptome profiling implied a tight relationship of AMI1 with plant stress responses. Intriguingly, the genetic perturbations of *AMI1* expression had strong impact on gene expression regulatory processes. Pathway analysis using the MapMan tool (Thimm *et al.*, 2004) highlighted that AP2/ERF-, MYB-, and WRKY-class transcription factors were among the most affected molecular components associated with the regulation of transcription (Supplementary Table S3). This likely suggests a role for IAM, or one of its derivatives, as a signaling molecule.

The ami1 *mutants are hypersensitive to osmotic stress and accumulate ABA*

Transcriptome profiling of *ami1-2* implicated a possible connection of IAM accumulation with abiotic stress responses. To gain additional insights into how AMI1 could be involved in plant stress responses, we examined the transcriptional response of *AMI1* towards different abiotic stress conditions (Fig. 7). While drought stress and salinity had either no or very little impact on *AMI1* expression, the osmotic stress treatment strongly repressed the expression of *AMI1* (Fig. 7B). To further characterize salinity and osmotic stress responses in *ami1*, we analysed the growth behavior of mutant and WT seedlings under stress conditions. The survival rate of the seedlings was assessed on the basis of first leaf emergence. When grown on 100 mM NaCl, *ami1* seedlings showed no considerable difference from WT. However, under osmotic stress conditions the survival rate of *ami1* seedlings was clearly reduced (Fig. 7A). The hypersensitivity of *ami1* seedlings towards osmotic stress conditions implies that the controlled repression of *AMI1* expression under osmotic stress conditions is an important mechanism in the stress adaptation process.

Osmotic stress responses are mediated by ABA-dependent and ABA-independent pathways (Agarwal *et al.*, 2006; Yoshida *et al.*, 2014). The microarray data underpinned the activation

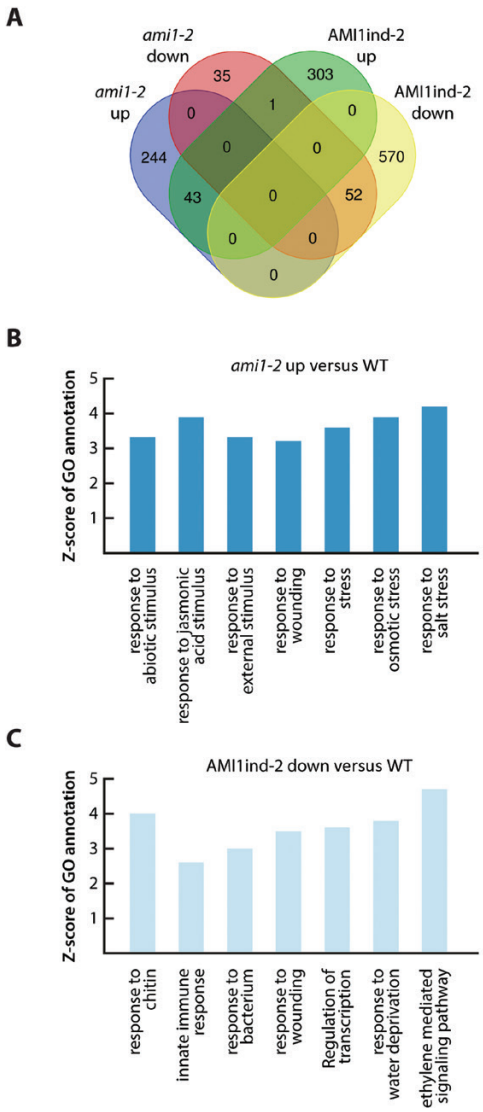

Fig. 6. Transcriptome changes in ami1-2 and AMI1ind-2 are consistent with a contribution to plant stress responses. (A) Venn diagram visualizing the overlap between transcripts de-regulated in *ami1-2* and AMI1ind-2. Only genes showing a congruent directional change in transcript levels were scored as overlapping. (B) The top seven over-represented GO annotations for biological processes according to parametric analysis of gene set enrichment (PAGE) of the selected genes up-regulated in *ami1-2*. (C) The top seven under-represented GO annotations for biological processes according to PAGE of the selected genes down-regulated in AMI1ind-2. The *Z*-scores show significant over/under-representation (Hochberg multiple testing adjustments in PAGE; $P<0.05$). Fold changes of all entities were determined in 12-day-old *ami1-2* and AMI1ind-2 versus wild-type seedlings, respectively.

of both pathways through the transcriptional regulation of key genes such as *NCED3* as well as several *MYB* and *DREB* class transcription factor genes, respectively. Dioxygenases of the NCED family catalyse a rate-limiting step of ABA biosynthesis. Mass spectrometric assessment of ABA levels in WT and *ami1* mutants revealed significantly increased hormone levels in the mutants (Fig. 7C). To investigate whether *NECD3* expression is responsive to ABA or to IAM, the transcriptional response of the gene was analysed by qPCR. Both substances induced *NCED3* expression (Fig. 7D). However, the observed effects were stronger in WT compared with mutant seedlings. Most interestingly, IAM showed a stronger effect in WT seedlings relative to ABA, which suggests that IAM acts either in parallel to ABA or upstream of the hormone in the transcriptional regulation of *NCED3*. Since *AMI1* gene expression was shown to be regulated by osmotic stress, we asked whether ABA could be involved in controlling *AMI1* expression in a feedback loop. On the basis of qPCR experiments and the quantification of promoter activity in *pAMI1::GUS* lines, we were not able to detect any regulatory effect of ABA on the expression of *AMI1* (see Supplementary Fig. S6).

Impaired AMI1 *expression translates into decreased seed and embryo size*

ABA is a major determinant of seed dormancy and germination (Vishal and Kumar, 2018). For this reason, we tested the effect of IAM on seed germination in comparison with ABA. Wild-type seeds were germinated on ½ MS plates containing methanol (mock), 10 µM IAM or ABA (Fig. 7E). As expected, ABA blocked seed germination nearly completely. Relative to the mock control, IAM also retarded the emergence of the radicle, most likely through the previously described induction of *NCED3* expression and the therewith coupled increase in ABA levels. A recent study reported the specific role of the KUP/HAK/KT-family K^+ transporter KUP9 in controlling cellular auxin homeostasis through the symport of IAA from the endoplasmic reticulum into the cytoplasm (Zhang *et al.*, 2020). Work from our lab related IAA and IAM with potassium influx in Arabidopsis embryos through the transcriptional control of K^+ transporter gene expression. The work also associated the two indolic compounds with the control of the seed size (Tenorio-Berrio *et al.*, 2018). In order to gain detailed information on the *ami1* mutant seed phenotype, we inspected seed and embryo size of *ami1* loss-of-function mutants in comparison with WT (Fig. 7F, G). The seed size of both *ami1* mutant alleles was significantly reduced. Consistent with this finding, the embryos of the *ami1* mutants were also observed to be considerably smaller. Overall, the presented data suggest that IAM triggers ABA production through the stimulation of its biosynthesis. Furthermore, it can be concluded that the accumulation of IAM in the *ami1* mutants exerts a negative effect on seed maturation.

Discussion

AMI1 contributes to auxin homeostasis in vivo

Auxins are well-characterized plant growth regulators ubiquitously distributed throughout the plant kingdom. Despite

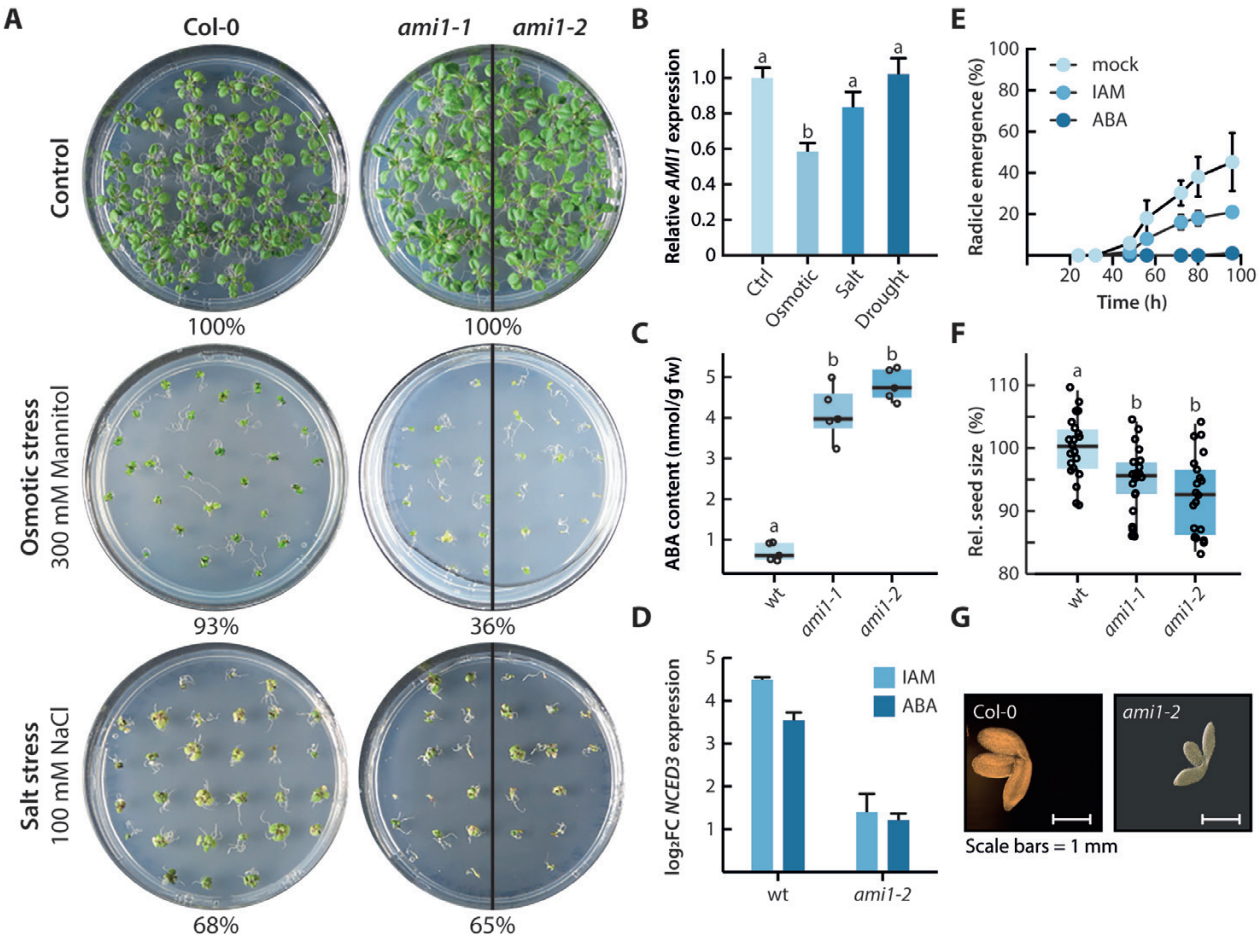

Fig. 7. Relationship between *AMI1* expression levels and ABA. (A) Abiotic stress assay growing control plants (Col-0) and *ami1* mutants for 12 d under control, salt (100 mM NaCl), and osmotic stress (300 mM mannitol) conditions. Stress resistance was assayed on the basis of first true leaf establishment. Qualitative data are given in the figure. (B) Transcriptional changes in *AMI1* expression in response to different stress treatments in comparison to control conditions. Gene expression levels were normalized to the house-keeping gene *APT1* using the $2^{-\Delta\Delta CT}$ method. Given are the means with their SE (n=9). (C) GC-MS/MS quantification of ABA contents in wild-type (WT) Arabidopsis and the two *ami1* mutant alleles. The box plots display the median, quartiles and extremes of the compared data sets (n=5). (D) Induction of *NCED3* gene expression by 10 µM IAM and ABA in wild-type (WT) and *ami1-2* seedlings, respectively. Gene expression levels were normalized to the house-keeping gene *APT1* using the $2^{-\Delta\Delta CT}$ method. Means with their SE are given (n=9). (E) Effect of either 10 µM ABA or IAM on the germination of WT Arabidopsis seeds. The germination rate was analysed on the basis of radicle emergence. Means with their SE are given (n=20). (F) Relative seed size of WT Arabidopsis and *ami1* mutant seeds. To analyse the seed size, seeds were photographed and the perimeter of at least 20 seeds determined using the Fiji software (Schindelin *et al.*, 2012). Different letters indicate significant differences between the means of the compared datasets analysed by ANOVA and a Tukey–Kramer *post hoc* test (P<0.05). (G) Size difference of representative WT (Col-0) and *ami1* mutant embryos. The photographs are scaled to the same size and scale bars (1 mm) are given.

considerable scientific interest in this substance class, our knowledge of IAA biosynthesis and cellular homeostasis in plants is still incomplete. The formation of IAA is assumed to proceed via several independent pathways that act either redundantly or in parallel to each other (Woodward and Bartel, 2005; Pollmann *et al.*, 2006*a*; Zhao, 2010). However, only the major auxin biosynthesis pathway via indole-3-pyruvate is yet fully uncovered with respect to the enzymes and intermediates involved (Zhao, 2014; Kasahara, 2016). Among the discussed additional pathways, one is suggested to proceed via IAM, which is further converted by IAM hydrolases to give rise to the active plant hormone, IAA. In recent years, evidence for the wide distribution of corresponding IAM hydrolases in the plant kingdom has been provided (Pollmann *et al.*, 2003; Nemoto *et al.*, 2009; Sánchez-Parra *et al.*, 2014), suggesting a conserved function of AMI1-like IAM hydrolases in plants. Here, we report the detailed characterization of *AMI1* loss- and gain-of-function mutants and show that AMI1 contributes to the conversion of IAM into IAA *in planta* (Figs 4–5; Supplementary Figs S2–S4). Remarkably, IAM hydrolase activity was not null in *ami1-1* and *ami1-2* (Fig. 4D), which suggested the existence of other enzymes that might be involved in the conversion of IAM into IAA, but the analysis of the other members of the amidase signature (AS) family in Arabidopsis provided no indication for a second specific IAM hydrolase in this group (Pollmann *et al.*, 2006*b*; Neu *et al.*, 2007). A recent

study, however, associated two additional formamidase-like proteins, IAMH1 and IAMH2, with this reaction (Gao *et al.*, 2020), which is likely the reason for the remaining enzymatic activity. It will be highly interesting to introgress the *ami1* mutation into the *iamh1 iamh2* CRISPR/Cas line in a future project, in order to fully understand the role of IAM in plants.

The IAM pathway is not essential for general IAA supply

The analysis of the root system architecture of *ami1-1* and *ami1-2* revealed significant differences in the specific root branch density, as well as the specific root area and length (see Supplementary Fig. S2). *AMI1* expression in primary roots declined shortly after germination (Fig. 2), but apparently a tight regulation of the spatio-temporal distribution of AMI1 is important to facilitate proper root growth. On the contrary, the conditional overexpression of AMI1 had no significant effect on root growth (Supplementary Fig. S2). Taking the increased response of AMI1ind lines towards exogenously applied IAM into account (Fig. 5), this implies that the IAM pool size in roots is low or not accessible for recombinant AMI1. Our observation is consistent with the lack of any considerable root phenotype when the *iaaM* and *iaaH* genes from *Agrobacterium tumefaciens* are expressed under the control of their natural promotors in Arabidopsis (van der Graaff *et al.*, 2003). Apparently, the IAM pool in areal plant parts must be bigger or more accessible to recombinant AMI1, as the leaves of AMI1ind plants showed clear phenotypic alterations (Supplementary Fig. S3) that can be associated with auxin overproduction, resembling the phenotypes of mutants such as *yuc1-D* (Zhao *et al.*, 2001) or the *sur2* mutant (Delarue *et al.*, 1998), although the effects in the AMI1ind lines are somewhat weaker.

However, on a whole-plant scale, the phenotypic alterations caused by mutations in *AMI1* are only moderate (Fig. 4; Supplementary Fig. S2), and the transcriptomics analysis of *ami1-2* did not provide evidence for a consistent induction of genes involved in other auxin biosynthesis pathways, and nor are *IAMH1* or *IAMH2* induced to compensate the lack of AMI1 in the mutant (Supplementary Table S2). Hence, it must be concluded that the IAM pathway is not strictly necessary for the general supply of IAA in Arabidopsis, although some particular developmental processes, such as lateral root growth or seed maturation (Fig. 7), may depend on AMI1 action to achieve full effectiveness.

Transcriptomics analyses revealed a link between AMI1 and plant stress responses

Our expression analyses demonstrated that *AMI1* transcription is differentially regulated by IAM and IAA, even though IAA appeared to be less effective controlling *AMI1* expression (Fig. 3). This further suggested a tight transcriptional connection between AMI1 and both its substrate and reaction product. Most interesting, however, was the observation that the genetic reduction of AMI1 levels caused no major alterations of auxin homeostasis-related gene expression. This contrasts with the results obtained for the conditional *AMI1* overexpression line. Here, the induction of a few auxin conjugation-related genes suggested the activation of compensatory effects, likely triggered to counteract auxin overproduction in the line (see Supplementary Table S2).

The comprehensive profiling of transcriptional alterations in *AMI1* mutants revealed a strong impact on genes related with biotic and abiotic stress responses, including key enzymes for the biosynthesis of JA and ABA (Fig. 6; see Supplementary Tables S2, S3). Along with numerous marker genes for ABA signaling, e.g. *RD26A*, *COR47*, *ERD4*, *ERD9*, and *ERD10*, the gene for a key-enzyme of ABA synthesis, *NCED3*, appeared strongly induced in *ami1-2*. The overexpression of *NCED3* has recently been associated with an improvement of drought tolerance in soybean (Molinari *et al.*, 2020). Both the induction of *NCED3* through IAM application and the accumulation of ABA in the *ami1* alleles could be confirmed (Fig. 7C, D), which provided strong arguments for an intimate relationship between AMI1 and IAM contents, respectively, and ABA. The considerable induction of AP2/ERF transcription factors in *ami1-2* (Supplementary Table S3) has to be particularly emphasized, as it underpins our observations of a close connection between AMI1 action and abiotic stress responses. The particular role of AP2/ERF transcription factor networks in orchestrating hormone and abiotic stress responses is well documented (Xie *et al.*, 2019). Quantitative gene expression analysis revealed a significant suppression of *AMI1* transcription by osmotic stress (Fig. 7B), and *ami1* mutants grown under osmotic stress conditions show a considerably increased sensitivity to the stress conditions (Fig. 7A). In consequence, we conclude that the suppression of *AMI1* expression by osmotic stress and the therewith linked accumulation of IAM are important variables that contribute to the fine-tuning of ABA-governed stress responses by triggering NCED3-mediated ABA biosynthesis in Arabidopsis.

ABA and gibberellins are essential determinants of seed development and dormancy (Carrera-Castaño *et al.*, 2020). A recent publication also highlighted a direct role of auxin in seed dormancy (Matilla, 2020). In addition, crosstalk between IAA and ABA in seed development and germination has been reported to occur on both the transcriptional and the metabolic level (Chauffour *et al.*, 2019; He *et al.*, 2020). With respect to our data on seed development and germination (Fig. 7E–G), it can be concluded that the crosstalk between AMI1/IAM contents and ABA-related processes is also involved in facilitating proper seedling development and germination. We were able to demonstrate that IAM application reduces the germination rate in Arabidopsis, likely through the induction of ABA biosynthesis. Moreover, mutations in *AMI1* translated into aberrant embryo and seed size.

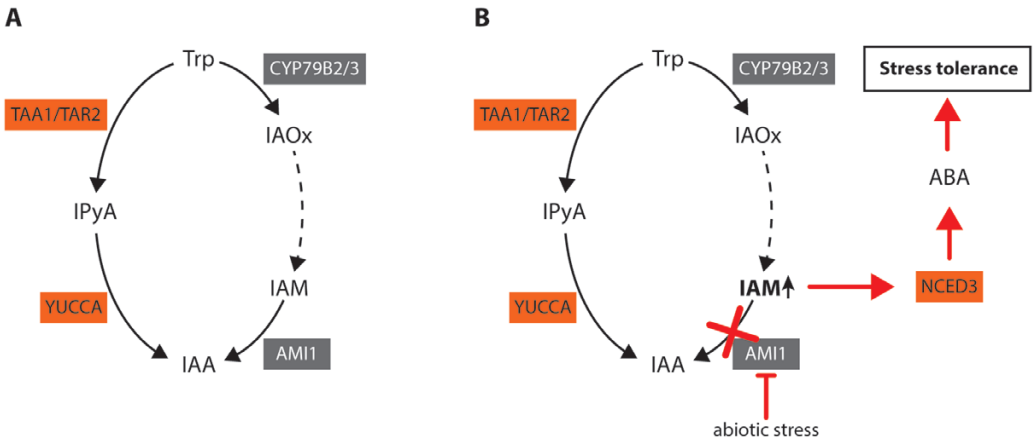

Fig. 8. Integrated model of the molecular role of AMI1. (A) Our data suggest that the metabolic flux of the parallel pathways normally leads without distortions to IAA. In this scenario, IAM does not accumulate considerably as it is quickly converted into IAA. (B) Under stress conditions, however, the expression of *AMI1* is repressed. In consequence, this results in the accumulation of IAM. The increasing IAM levels gradually induce the expression of *NCED3* and trigger the subsequent biosynthesis of ABA as well as the corresponding downstream processes that confer stress resistance in Arabidopsis.

The Arabidopsis AS superfamily member FATTY ACID AMIDE HYDROLASE (FAAH) is associated with numerous developmental processes, including plant growth and early flowering, and interacts with ABA signaling (Wang *et al.*, 2006; Teaster *et al.*, 2007, 2012). FAAH catalyses the hydrolysis of *N*-acylethanolamines, lipid signaling molecules that orchestrate a wide array of physiological processes in multicellular eukaryotes (Chapman, 2004), which terminates their action (Aziz and Chapman, 2020). Although there are marked differences between FAAH and AMI1 with respect to their substrate preferences (Pollmann *et al.*, 2006*b*), the growth inhibiting properties of their preferred substrates led us to the hypothesis that the main role of AMI1 might be similar to that of FAAH, i.e. terminating the action of IAM through its conversion to free IAA and NH_4^+. Particularly in plant stress responses and seed development, this mechanism involving the IAM-induced biosynthesis of ABA (Fig. 8) seems to be important to drive proper adaptational responses. In consequence, the AMI1-dependent metabolic flux through the IAM shunt is seemingly an important regulatory variable that connects auxin-mediated plant growth processes with plant stress responses. It will be highly interesting to further investigate the regulatory role of IAM in plants and how the corresponding signal is perceived and translated into downstream responses. At the same time, it appears tempting to us to further investigate the transcriptional networks that are involved in the integration of the IAM signal.

Supplementary data

Supplementary data are available at *JXB* online.

Fig. S1. Expression analysis of *AMI1* in WT and genotyping of *ami1* alleles.

Fig. S2. Root phenotype of *AMI1* mutant plants.

Fig. S3. Phenotype of conditionally *AMI1* overexpressing AMI1ind lines.

Fig. S4. Root growth responses of conditional *AMI1* overexpression lines towards IAM and IAA in the media.

Fig. S5. Validation of microarray data by qRT-PCR, related to Fig. 6.

Fig. S6. Effect of ABA on *AMI1* gene expression.

Table S1. Primers used for genotyping, cloning and expression analysis.

Table S2. Microarray analysis.

Table S3. GO and MapMan analysis of selected up- and down-regulated genes in the *AMI1* mutants.

Acknowledgements

The authors thank the NASC for providing seeds of T-DNA insertion and mutant lines, and Prof. Nam-Hai Chua (The Rockefeller University, New York) for providing the pMDC7 vector. Moreover, SP is grateful to Prof. Elmar W. Weiler (Ruhr-Universität Bochum, Germany) for his support in the initial phase of the AMI1 project. This research was supported by grants from the German Research Foundation (DFG, SFB480/A10) and the Spanish Ministry of Economy, Industry and Competitiveness (MINECO, BFU2017-82826-R to SP and a grant from the Swedish Research Council (VR) to HA. JM was supported by the 'Severo Ochoa Program for Centers of Excellence in R&D' from the Agencia Estatal de Investigación of Spain, grant SEV-2016-0672 (2017-2021) to the CBGP.

Conflict of interest

The authors declare no conflict of interests

Author contributions

SP and MDW conceptualized the project and were responsible for acquiring the funding; MMPA, POG, JMC, TL, BSP, RGB, SK, MRA, HA,

and SP performed the experiments; MMPA, RGB, HA, MDW, and SP analysed and interpreted the data; SP wrote the paper with significant input from all other authors.

Data availability

All data supporting the findings of this study are available within the paper and within its supplementary data published online.

References

Agarwal PK, Agarwal P, Reddy MK, Sopory SK. 2006. Role of DREB transcription factors in abiotic and biotic stress tolerance in plants. Plant Cell Reports **25**, 1263–1274.

Alonso JM, Stepanova AN, Leisse TJ, *et al.* 2003. Genome-wide insertional mutagenesis of *Arabidopsis thaliana*. Science **301**, 653–657.

Aronsson H, Boij P, Patel R, Wardle A, Töpel M, Jarvis P. 2007. Toc64/OEP64 is not essential for the efficient import of proteins into chloroplasts in *Arabidopsis thaliana*. The Plant Journal **52**, 53–68.

Aziz M, Chapman KD. 2020. Fatty acid amide hydrolases: An expanded capacity for chemical communication? Trends in Plant Science **25**, 236–249.

Becker D, Kemper E, Schell J, Masterson R. 1992. New plant binary vectors with selectable markers located proximal to the left T-DNA border. Plant Molecular Biology **20**, 1195–1197.

Björk RG, Majdi H, Klemedtsson L, Lewis-Jonsson L, Molau U. 2007. Long-term warming effects on root morphology, root mass distribution, and microbial activity in two dry tundra plant communities in northern Sweden. New Phytologist **176**, 862–873.

Bradford MM. 1976. A rapid and sensitive method for the quantitation of microgram quantities of protein utilizing the principle of protein-dye binding. Analytical Biochemistry **72**, 248–254.

Brumos J, Robles LM, Yun J, Vu TC, Jackson S, Alonso JM, Stepanova AN. 2018. Local auxin biosynthesis is a key regulator of plant development. Developmental Cell **47**, 306–318.e5.

Carrera-Castaño G, Calleja-Cabrera J, Pernas M, Gómez L, Oñate-Sánchez L. 2020. An updated overview on the regulation of seed germination. Plants **9**, 703.

Chapman KD. 2004. Occurrence, metabolism, and prospective functions of *N*-acylethanolamines in plants. Progress in Lipid Research **43**, 302–327.

Chauffour F, Bailly M, Perreau F, *et al.* 2019. Multi-omics analysis reveals sequential roles for ABA during seed maturation. Plant Physiology **180**, 1198–1218.

Claeys H, Inzé D. 2013. The agony of choice: how plants balance growth and survival under water-limiting conditions. Plant Physiology **162**, 1768–1779.

Clough SJ, Bent AF. 1998. Floral dip: a simplified method for *Agrobacterium*-mediated transformation of *Arabidopsis thaliana*. The Plant Journal **16**, 735–743.

Czechowski T, Stitt M, Altmann T, Udvardi MK, Scheible WR. 2005. Genome-wide identification and testing of superior reference genes for transcript normalization in Arabidopsis. Plant Physiology **139**, 5–17.

Davies PJ. 2010. Plant hormones. Biosynthesis, signal transduction, action! Dordrecht: Springer Netherlands.

Davies RT, Goetz DH, Lasswell J, Anderson MN, Bartel B. 1999. *IAR3* encodes an auxin conjugate hydrolase from Arabidopsis. The Plant Cell **11**, 365–376.

Delarue M, Prinsen E, Onckelen HV, Caboche M, Bellini C. 1998. *Sur2* mutations of *Arabidopsis thaliana* define a new locus involved in the control of auxin homeostasis. The Plant Journal **14**, 603–611.

Depuydt S, Hardtke CS. 2011. Hormone signalling crosstalk in plant growth regulation. Current Biology **21**, R365–R373.

Evan GI, Lewis GK, Ramsay G, Bishop JM. 1985. Isolation of monoclonal antibodies specific for human *c-myc* proto-oncogene product. Molecular and Cellular Biology **5**, 3610–3616.

Gallagher SR. 1992. Quantitation of GUS activity by fluorometry. In: Gallagher SR, ed. GUS protocols: using the GUS gene as a reporter of gene expression. New York: Academic Press, 47–59.

Gao Y, Dai X, Aoi Y, Takebayashi Y, Yang L, Guo X, Zeng Q, Yu H, Kasahara H, Zhao Y. 2020. Two homologous *INDOLE-3-ACETAMIDE (IAM) HYDRALASE* genes are required for the auxin effects of IAM in *Arabidopsis*. Journal of Genetics and Genomics **47**, 157–165

Gélinas-Marion A, Nichols DS, Ross JJ. 2020. Conversion of unstable compounds can contribute to the auxin pool during sample preparation. Plant Physiology **183**, 1432–1434.

Gomez-Cadenas A, Vives V, Zandalinas SI, Manzi M, Sanchez-Perez AM, Perez-Clemente RM, Arbona V. 2015. Abscisic acid: a versatile phytohormone in plant signaling and beyond. Current Protein & Peptide Science **16**, 413–434.

He Y, Zhao J, Yang B, Sun S, Peng L, Wang Z. 2020. Indole-3-acetate beta-glucosyltransferase *OsIAGLU* regulates seed vigour through mediating crosstalk between auxin and abscisic acid in rice. Plant Biotechnology Journal **18**, 1933–1945.

Hentrich M, Böttcher C, Düchting P, Cheng Y, Zhao Y, Berkowitz O, Masle J, Medina J, Pollmann S. 2013. The jasmonic acid signaling pathway is linked to auxin homeostasis through the modulation of *YUCCA8* and *YUCCA9* gene expression. The Plant Journal **74**, 626–637.

Hoffmann M, Lehmann T, Neu D, Hentrich M, Pollmann S. 2010. Expression of *AMIDASE1* (*AMI1*) is suppressed during the first two days after germination. Plant Signaling & Behavior **5**, 1642–1644.

Jefferson RA, Kavanagh TA, Bevan MW. 1987. GUS fusions: beta-glucuronidase as a sensitive and versatile gene fusion marker in higher plants. The EMBO Journal **6**, 3901–3907.

Jost R, Berkowitz O, Masle J. 2007. Magnetic quantitative reverse transcription PCR: a high-throughput method for mRNA extraction and quantitative reverse transcription PCR. BioTechniques **43**, 206–211.

Julkowska MM, Testerink C. 2015. Tuning plant signaling and growth to survive salt. Trends in Plant Science **20**, 586–594.

Karlin-Neumann GA, Brusslan JA, Tobin EM. 1991. Phytochrome control of the *tms2* gene in transgenic *Arabidopsis*: a strategy for selecting mutants in the signal transduction pathway. The Plant Cell **3**, 573–582.

Kasahara H. 2016. Current aspects of auxin biosynthesis in plants. Bioscience, Biotechnology, and Biochemistry **80**, 34–42.

Kazan K, Manners JM. 2013. MYC2: the master in action. Molecular Plant **6**, 686–703.

Kim SY, Volsky DJ. 2005. PAGE: parametric analysis of gene set enrichment. BMC Bioinformatics **6**, 144.

LeClere S, Tellez R, Rampey RA, Matsuda SP, Bartel B. 2002. Characterization of a family of IAA-amino acid conjugate hydrolases from *Arabidopsis*. The Journal of Biological Chemistry **277**, 20446–20452.

Lehmann T, Janowitz T, Sánchez-Parra B, Alonso MP, Trompetter I, Piotrowski M, Pollmann S. 2017. Arabidopsis NITRILASE 1 contributes to the regulation of root growth and development through modulation of auxin biosynthesis in seedlings. Frontiers in Plant Science **8**, 36.

Lewis DR, Olex AL, Lundy SR, Turkett WH, Fetrow JS, Muday GK. 2013. A kinetic analysis of the auxin transcriptome reveals cell wall remodeling proteins that modulate lateral root development in *Arabidopsis*. The Plant Cell **25**, 3329–3346.

Livak KJ, Schmittgen TD. 2001. Analysis of relative gene expression data using real-time quantitative PCR and the $2^{-\Delta\Delta C(T)}$ method. Methods **25**, 402–408.

Ljung K. 2013. Auxin metabolism and homeostasis during plant development. Development **140**, 943–950.

Ma Y, Cao J, He J, Chen Q, Li X, Yang Y. 2018. Molecular mechanism for the regulation of ABA homeostasis during plant development and stress responses. International Journal of Molecular Sciences **19**, 3643.

Maere S, Heymans K, Kuiper M. 2005. BiNGO: a Cytoscape plugin to assess overrepresentation of gene ontology categories in biological networks. Bioinformatics **21**, 3448–3449.

Matilla AJ. 2020. Auxin: Hormonal signal required for seed development and dormancy. Plants **9**, 705.

Molinari MDC, Fuganti-Pagliarini R, Marin SRR, *et al.* 2020. Overexpression of *AtNCED3* gene improved drought tolerance in soybean in greenhouse and field conditions. Genetics and Molecular Biology **43**, e20190292.

Murashige T, Skoog F. 1962. A revised medium for rapid growth and bio assays with tobacco tissue cultures. Physiologia Plantarum **15**, 473–497.

Nemoto K, Hara M, Suzuki M, Seki H, Muranaka T, Mano Y. 2009. The *NtAMI1* gene functions in cell division of tobacco BY-2 cells in the presence of indole-3-acetamide. FEBS Letters **583**, 487–492.

Neu D, Lehmann T, Elleuche S, Pollmann S. 2007. *Arabidopsis* amidase 1, a member of the amidase signature family. The FEBS Journal **274**, 3440–3451.

Nolan TM, Brennan B, Yang M, Chen J, Zhang M, Li Z, Wang X, Bassham DC, Walley J, Yin Y. 2017. Selective autophagy of BES1 mediated by DSK2 balances plant growth and survival. Developmental Cell **41**, 33–46.e7.

Novák O, Hényková E, Sairanen I, Kowalczyk M, Pospíšil T, Ljung K. 2012. Tissue-specific profiling of the *Arabidopsis thaliana* auxin metabolome. The Plant Journal **72**, 523–536.

Okushima Y, Mitina I, Quach HL, Theologis A. 2005. AUXIN RESPONSE FACTOR 2 (ARF2): a pleiotropic developmental regulator. The Plant Journal **43**, 29–46.

Oñate-Sánchez L, Vicente-Carbajosa J. 2008. DNA-free RNA isolation protocols for *Arabidopsis thaliana*, including seeds and siliques. BMC Research Notes **1**, 93.

Perdomo JA, Conesa MÀ, Medrano H, Ribas-Carbó M, Galmés J. 2015. Effects of long-term individual and combined water and temperature stress on the growth of rice, wheat and maize: relationship with morphological and physiological acclimation. Physiologia Plantarum **155**, 149–165.

Pinon V, Prasad K, Grigg SP, Sanchez-Perez GF, Scheres B. 2013. Local auxin biosynthesis regulation by PLETHORA transcription factors controls phyllotaxis in *Arabidopsis*. Proceedings of the National Academy of Sciences, USA **110**, 1107–1112.

Pollmann S, Müller A, Piotrowski M, Weiler EW. 2002. Occurrence and formation of indole-3-acetamide in *Arabidopsis thaliana*. Planta **216**, 155–161.

Pollmann S, Müller A, Weiler EW. 2006*a*. Many roads lead to "auxin": of nitrilases, synthases, and amidases. Plant Biology **8**, 326–333.

Pollmann S, Neu D, Lehmann T, Berkowitz O, Schäfer T, Weiler EW. 2006*b*. Subcellular localization and tissue specific expression of amidase 1 from *Arabidopsis thaliana*. Planta **224**, 1241–1253.

Pollmann S, Neu D, Weiler EW. 2003. Molecular cloning and characterization of an amidase from *Arabidopsis thaliana* capable of converting indole-3-acetamide into the plant growth hormone, indole-3-acetic acid. Phytochemistry **62**, 293–300.

Ramos P, Rivas N, Pollmann S, Casati P, Molina-Montenegro MA. 2018. Hormonal and physiological changes driven by fungal endophytes increase Antarctic plant performance under UV-B radiation. Fungal Ecology **34**, 76–82.

Ritchie ME, Phipson B, Wu D, Hu Y, Law CW, Shi W, Smyth GK. 2015. limma powers differential expression analyses for RNA-sequencing and microarray studies. Nucleic Acids Research **43**, e47.

Ruiz Rosquete M, Barbez E, Kleine-Vehn J. 2012. Cellular auxin homeostasis: gatekeeping is housekeeping. Molecular Plant **5**, 772–786.

Sánchez-Parra B, Frerigmann H, Alonso MM, Loba VC, Jost R, Hentrich M, Pollmann S. 2014. Characterization of four bifunctional plant IAM/PAM-amidohydrolases capable of contributing to auxin biosynthesis. Plants **3**, 324–347.

Schindelin J, Arganda-Carreras I, Frise E, *et al.* 2012. Fiji: an open-source platform for biological-image analysis. Nature Methods **9**, 676–682.

Silva EN, Vieira SA, Ribeiro RV, Ponte LFA, Ferreira-Silva SL, Silveira JAG. 2013. Contrasting physiological responses of *Jatropha curcas* plants to single and combined stresses of salinity and heat. Journal of Plant Growth Regulation **32**, 159–169.

Sitbon F, Hennion S, Sundberg B, Little CH, Olsson O, Sandberg G. 1992. Transgenic tobacco plants coexpressing the *Agrobacterium tumefaciens iaaM* and *iaaH* genes display altered growth and indoleacetic acid metabolism. Plant Physiology **99**, 1062–1069.

Smyth DR, Bowman JL, Meyerowitz EM. 1990. Early flower development in *Arabidopsis*. The Plant Cell **2**, 755–767.

Spoel SH, Dong X. 2008. Making sense of hormone crosstalk during plant immune responses. Cell Host & Microbe **3**, 348–351.

Staswick PE, Serban B, Rowe M, Tiryaki I, Maldonado MT, Maldonado MC, Suza W. 2005. Characterization of an Arabidopsis enzyme family that conjugates amino acids to indole-3-acetic acid. The Plant Cell **17**, 616–627.

Sugawara S, Hishiyama S, Jikumaru Y, Hanada A, Nishimura T, Koshiba T, Zhao Y, Kamiya Y, Kasahara H. 2009. Biochemical analyses of indole-3-acetaldoxime-dependent auxin biosynthesis in *Arabidopsis*. Proceedings of the National Academy of Sciences, USA **106**, 5430–5435.

Sun J, Xu Y, Ye S, *et al.* 2009. *Arabidopsis ASA1* is important for jasmonate-mediated regulation of auxin biosynthesis and transport during lateral root formation. The Plant Cell **21**, 1495–1511.

Suzuki N, Rivero RM, Shulaev V, Blumwald E, Mittler R. 2014. Abiotic and biotic stress combinations. New Phytologist **203**, 32–43.

Teaster ND, Keereetaweep J, Kilaru A, Wang YS, Tang Y, Tran CN, Ayre BG, Chapman KD, Blancaflor EB. 2012. Overexpression of fatty acid amide hydrolase induces early flowering in *Arabidopsis thaliana*. Frontiers in Plant Science **3**, 32.

Teaster ND, Motes CM, Tang Y, *et al.* 2007. *N*-Acylethanolamine metabolism interacts with abscisic acid signaling in *Arabidopsis thaliana* seedlings. The Plant Cell **19**, 2454–2469.

Tenorio-Berrio R, Pérez-Alonso MM, Vicente-Carbajosa J, Martin-Torres L, Dreyer I, Pollmann S. 2018. Identification of two auxin-regulated potassium transporters involved in seed maturation. International Journal of Molecular Sciences **19**, 2132.

Thimm O, Bläsing O, Gibon Y, Nagel A, Meyer S, Krüger P, Selbig J, Müller LA, Rhee SY, Stitt M. 2004. MAPMAN: a user-driven tool to display genomics data sets onto diagrams of metabolic pathways and other biological processes. The Plant Journal **37**, 914–939.

Truman WM, Bennett MH, Turnbull CG, Grant MR. 2010. Arabidopsis auxin mutants are compromised in systemic acquired resistance and exhibit aberrant accumulation of various indolic compounds. Plant Physiology **152**, 1562–1573.

van der Graaff E, Boot K, Granbom R, Sandberg G, Hooykaas PJJ. 2003. Increased endogenous auxin production in *Arabidopsis thaliana* causes both earlier described and novel auxin-related phenotypes. Journal of Plant Growth Regulation **22**, 240–252.

Vanneste S, Friml J. 2009. Auxin: a trigger for change in plant development. Cell **136**, 1005–1016.

Verma V, Ravindran P, Kumar PP. 2016. Plant hormone-mediated regulation of stress responses. BMC Plant Biology **16**, 86.

Vishal B, Kumar PP. 2018. Regulation of seed germination and abiotic stresses by gibberellins and abscisic acid. Frontiers in Plant Science **9**, 838.

Voß U, Bishopp A, Farcot E, Bennett MJ. 2014. Modelling hormonal response and development. Trends in Plant Science **19**, 311–319.

Wang YS, Shrestha R, Kilaru A, Wiant W, Venables BJ, Chapman KD, Blancaflor EB. 2006. Manipulation of *Arabidopsis* fatty acid amide hydrolase expression modifies plant growth and sensitivity to *N*-acylethanolamines. Proceedings of the National Academy of Sciences, USA **103**, 12197–12202.

Woodward AW, Bartel B. 2005. Auxin: regulation, action, and interaction. Annals of Botany **95**, 707–735.

Xie Z, Nolan TM, Jiang H, Yin Y. 2019. AP2/ERF transcription factor regulatory networks in hormone and abiotic stress responses in *Arabidopsis*. Frontiers in Plant Science **10**, 228.

Yoshida T, Mogami J, Yamaguchi-Shinozaki K. 2014. ABA-dependent and ABA-independent signaling in response to osmotic stress in plants. Current Opinion in Plant Biology **21**, 133–139.

Zhang ML, Huang PP, Ji Y, Wang S, Wang SS, Li Z, Guo Y, Ding Z, Wu WH, Wang Y. 2020. KUP9 maintains root meristem activity by regulating K^+ and auxin homeostasis in response to low K. EMBO Reports **21**, e50164.

Zhang Z, Li Q, Li Z, Staswick PE, Wang M, Zhu Y, He Z. 2007. Dual regulation role of *GH3.5* in salicylic acid and auxin signaling during Arabidopsis-*Pseudomonas syringae* interaction. Plant Physiology **145**, 450–464.

Zhao Y. 2010. Auxin biosynthesis and its role in plant development. Annual Review of Plant Biology **61**, 49–64.

Zhao Y. 2014. Auxin biosynthesis. The Arabidopsis Book **12**, e0173.

Zhao Y, Christensen SK, Fankhauser C, Cashman JR, Cohen JD, Weigel D, Chory J. 2001. A role for flavin monooxygenase-like enzymes in auxin biosynthesis. Science **291**, 306–309.

Zhao Y, Hull AK, Gupta NR, Goss KA, Alonso J, Ecker JR, Normanly J, Chory J, Celenza JL. 2002. Trp-dependent auxin biosynthesis in *Arabidopsis*: involvement of cytochrome P450s CYP79B2 and CYP79B3. Genes & Development **16**, 3100–3112.

Zhu JK. 2002. Salt and drought stress signal transduction in plants. Annual Review of Plant Biology **53**, 247–273.

Zimmerman PW, Hitchcock AE. 1942. Substituted phenoxy and benzoic acid growth substances and the relation of structure to physiological activity. Contributions of the Boyce Thompson Institute **12**, 321–343.

Zuo J, Niu QW, Chua NH. 2000. Technical advance: An estrogen receptor-based transactivator XVE mediates highly inducible gene expression in transgenic plants. The Plant Journal **24**, 265–273.